Nanoscale Advances

ROYAL SOCIETY OF CHEMISTRY

PAPER

View Article Online
View Journal | View Issue

Cite this: *Nanoscale Adv.*, 2021, **3**, 3107

Synergetic enhancement of thermoelectric performances by localized carrier and phonon scattering in Cu_2Se with incorporated fullerene nanoparticles†

Yingshi Jin,‡[a] Junphil Hwang,‡[a] Sujin Kim,[a] Jungwon Kim [b] and Sung-Jin Kim *[a]

Received 3rd February 2021
Accepted 7th April 2021

DOI: 10.1039/d1na00085c

rsc.li/nanoscale-advances

C_{60}/Cu_2Se thermoelectric nanocomposites were synthesized with various amounts of fullerene (C_{60}; 0.03, 0.3, 0.5, 0.7 mol%) incorporated in Cu_2Se. The thermoelectric figures of merits (zT) of the C_{60}/Cu_2Se nanocomposites were enhanced by 20–30% compared to that of pure Cu_2Se, reaching a value of 1.4 at 773 K. The primary cause of zT enhancement is the synergetic effect of thermal conductivity reduction by phonon scattering and Seebeck coefficient increase by carrier localization that results from incorporation of C_{60} nanoparticles. Theoretical calculations for Seebeck coefficient enhancement and lattice thermal conductivity reduction were performed. The Seebeck coefficients of C_{60}/Cu_2Se nanocomposites were around 43% higher than that of pure Cu_2Se, whereas the reduction of lattice thermal conductivity with incorporation of C_{60} was around 40–50%.

Introduction

Thermoelectric nanocomposites have powerful advantages with regard to overcoming the complex coupling of transport properties. A thermoelectric material can convert thermal energy to electrical energy and *vice versa*.[1] Thermoelectric conversion efficiency is a function of a dimensionless parameter known as the thermoelectric figure of merit, $zT = (S^2\sigma/\kappa)T$,[1] where S, σ, κ, and T are the Seebeck coefficient, electrical conductivity, thermal conductivity, and temperature, respectively.[1] Conversion efficiency increases with zT.[1] However, zT increase is difficult due to the coupling of three interdependent parameters that determine zT. The thermal conductivity, κ, is composed of electron and phonon contributions; thus, the thermal conductivity is coupled to electrical conductivity, σ. The Seebeck coefficient, S, is reversely coupled to electrical conductivity.[2] The Seebeck coefficient can be derived from the Boltzmann transport equation. According to quantum statistical mechanics, the Seebeck coefficient can be determined with the following equation:[2]

$$S = \frac{1}{eT}\frac{\int_0^\infty E\tau(E)(E-E_F)D(E)\frac{\partial f}{\partial E}\mathrm{d}E}{\int_0^\infty E\tau(E)D(E)\frac{\partial f}{\partial E}\mathrm{d}E} \quad (1)$$

where E, τ, D, and f are the electron energy, scattering time, density of states, and Fermi–Dirac distribution function, respectively. The denominator of eqn (1) is the electrical conductivity.[2] A nanocomposite with embedded nanoparticles can effectively scatter phonons reducing the lattice thermal conductivity.[3–5] Several studies[6–14,39,40] have reported that embedded nanoparticles in the form of precipitates can reduce lattice thermal conductivity and enhance the zT. Another useful effect of embedding nanoparticles is known as the energy filtering effect.[15,16] The numerator of eqn (1) can be rewritten as $\int A(E)(E-E_F)\mathrm{d}E$, where $A(E)$ is $E\tau(E)D(E)\partial f/\partial E$. Because the $E-E_F$ term has point symmetry at the Fermi level, E_F, it is important to enhance the asymmetry of $A(E)$ around the Fermi level to increase the Seebeck coefficient.[16] The derivative of Fermi–Dirac distribution ($\partial f/\partial E$) has perfect symmetry around the Fermi level, thus it is important to enhance the energy dependence of $\tau(E)$ and $D(E)$. The embedded nanoparticles have a different band structure from that of the matrix. Therefore, low energy conduction electrons could be scattered by a potential barrier or trapped by a potential well. In this study, the scattering time $\tau(E)$ due to impurity scattering induced by the incorporated C_{60} can be highly energy dependent,[16] a phenomenon known as the energy filtering effect. In our previous report,[17] embedded Au nanoparticles were shown to scatter electrons in a highly energy-dependent manner, resulting in the energy filtering effect and the Seebeck coefficient enhancement.

[a]*Department of Chemistry and Nano Science, Ewha Womans University, Seoul 03760, Korea. E-mail: sjkim@ewha.ac.kr*

[b]*Institute of Advanced Composite Materials, Korea Institute of Science and Technology (KIST), Jeonbuk 55324, Korea*

† Electronic supplementary information (ESI) available. See DOI: 10.1039/d1na00085c

‡ These authors equally contributed to this work.

Cu_2Se is an excellent thermoelectric material due to its PLEC (Phonon Liquid Electron Crystal) characteristic.[18] The superionic conduction of Cu ions with liquid-like mobility can reduce the shear resistance of Cu_2Se crystals, resulting in ultralow lattice thermal conductivity.[18–22] Recently, a graphene-incorporated Cu_2Se nanocomposite was reported.[23] The study demonstrated that clustered graphene–Cu_2Se mixtures could effectively reduce the lattice thermal conductivity.[23]

In this study, we found synergetic effects of embedding C_{60} in Cu_2Se to improve zT. The carrier localization (energy filtering effect) and phonon scattering caused by C_{60} nanoparticles effectively enhanced the Seebeck coefficient and reduced the lattice thermal conductivity. Fullerenes behave as semiconductors with a band gap around 1.5–5 eV[24,25] which is suitable for the formation of a potential well in a matrix of the p-type semiconductor of Cu_2Se with band gap around 1–2 eV. V. A. Kulbachinskii *et al.* have reported[26] that the electron acceptor behavior of C_{60} molecules increases the hole concentration in a BST (Bi–Sb–Te) alloy system. Meanwhile, D. Zhao *et al.* have reported[27] the energy filtering effect of embedded C_{60} in a Cu_2SnSe_3 system. In our study, we found that fullerenes act as potential wells to carriers and as scatterers to phonons. Theoretical calculations based on the Boltzmann transport equation for carrier localization clarifies that the source of Seebeck coefficient enhancement is formation of potential wells by embedded C_{60}.[2,15] Phonon scattering by fullerene nanoparticles in the Cu_2Se matrix is calculated using the model reported by W. Kim *et al.*[3,4,28,29]

Results & discussion

The C_{60}/Cu_2Se nanocomposites were prepared with various amounts of C_{60}; 0.03, 0.3, 0.5, 0.7 mol% incorporated in the Cu_2Se matrix. Due to the lower density of C_{60} compared to Cu_2Se, C_{60} molar percentages of 0.03, 0.3, 0.5, and 0.7% correspond to the higher volumetric percentages of approximately 0.5, 5, 8, and 10%, respectively. These C_{60} concentrations were used for phonon scattering calculations. From our previous report,[12] phonon scattering by embedded nanoparticles strongly depends on the interparticle distance between nanoparticles. To obtain optimal phonon scattering, the interparticle distances should be less than 15 nm.[12] Considering that the average size of C_{60} is around 1 nm, a rough estimation as described in the ESI (Table S1†) suggests that volumetric percentages around 1–10 vol% yield interparticle distances on the few nanometer scale. Even though we assumed that our nanoparticles consisted of clustered C_{60} in the fullerite form, the interparticle distances were estimated to be less than 15 nm (Table S1†). The microstructures of the fabricated samples are shown in Fig. 1. The resultant microstructures clearly differed for samples with varying C_{60} contents. When comparing pure Cu_2Se to the C_{60}/Cu_2Se nanocomposites, the most notable difference was average grain size. The grain size of pure Cu_2Se is a few micrometers. However, the grain sizes of the C_{60}/Cu_2Se nanocomposites are less than 100 nm, which seemed to be due to the Zener pinning effect.[30] When small incoherent particles are dispersed in a material, a counter force is applied against grain growth by the dispersed particles, which is known as the Zener pinning pressure.[31] For this reason, the grain growth of a C_{60}/Cu_2Se nanocomposite is interrupted, resulting in a smaller grain size than in pure Cu_2Se. D. Chen *et al.*[32] reported that the R/d ratio should be large to produce a strong Zener pinning pressure, where R is the particle size, and d is the interparticle distance. They reported that 0.4–0.8 nm sized particles

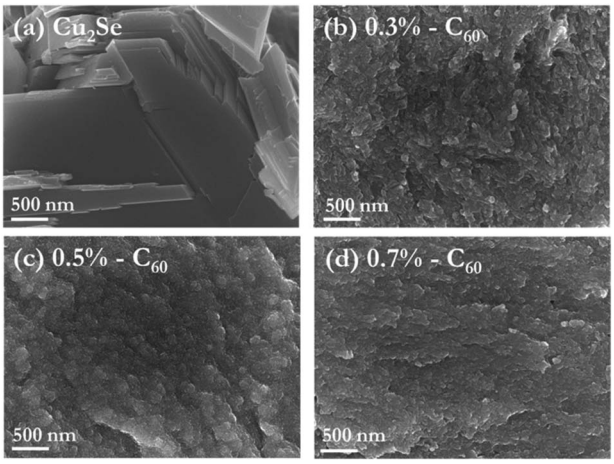

Fig. 1 SEM images of (a) pure Cu_2Se and nanocomposites of Cu_2Se embedded with (b) 0.3, (c) 0.5, and (d) 0.7 mol% C_{60}. Images (a–d) are produced at mid-magnification (×50 000).[38]

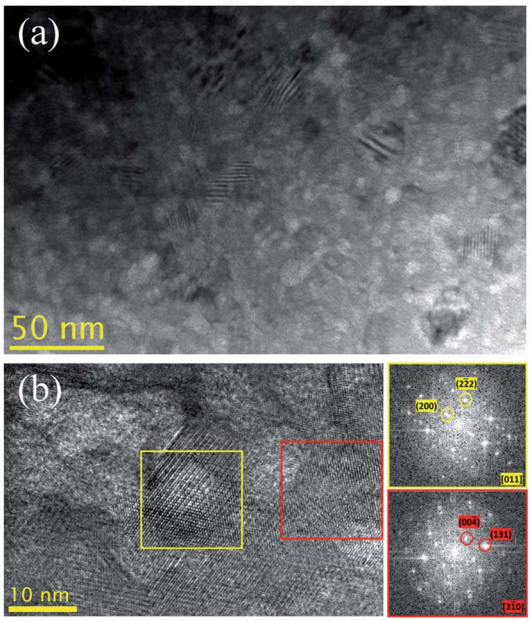

Fig. 2 (a) Low magnification and (b) high resolution TEM images of the 0.7 mol% C_{60}/Cu_2Se nanocomposite. The FFT pattern with a yellow border is obtained from a region of bright contrast (yellow box) and that with a red border is from a background region (red box).[38]

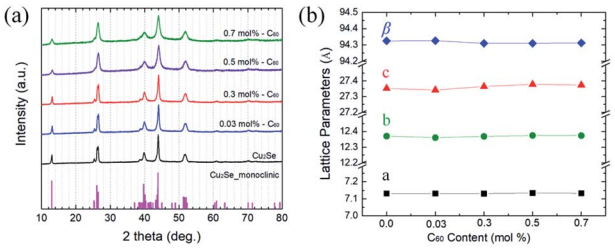

Fig. 3 (a) XRD data for pure Cu_2Se and C_{60}/Cu_2Se nanocomposites. (b) Lattice parameters for *a* (black), *b* (green), *c* (red) in the monoclinic unit cell, and angle β (blue).[38]

with 4–13 nm interparticle distance are sufficient to create the pinning effect.[32]

The dispersed C_{60} was analyzed in detail using transmission electron microscopy (TEM) as shown in Fig. 2. The low-magnification image shown in Fig. 2(a) shows that the 0.7 mol% C_{60}/Cu_2Se nanocomposite has a small grain size (below 50 nm) and a large number of bright contrast regions. The carbon atom is much lighter than Cu and Se, and C_{60} produces bright contrast in TEM images. The high resolution TEM (HR-TEM) image shown in Fig. 2(b) clearly indicates that the bright contrast region has a lattice spacing different from that of the Cu_2Se matrix. The fast Fourier transform (FFT) patterns showed that the bright contrast region contains lattice spacings of 7.42 and 4.46 Å, which correspond to the interplanar distance of the (200) and (2$\bar{2}$2) planes, indexed based on FCC fullerite, respectively.[33] On the other hand, the FFT pattern from the background shows lattice spacings of 6.84 and 3.52 Å, which correspond to the interplanar distance of the (00$\bar{4}$) and (131) planes of monoclinic α-Cu_2Se, respectively.[34] These results indicate that the C_{60}s incorporated in the Cu_2Se matrix are agglomerated in fullerite structures with sizes of 5–10 nm. The estimated interparticle distance is roughly 4–15 nm (Table S1†), which must be sufficient to produce the Zener pinning effect. XRD data and lattice parameters for each crystalline plane are plotted in Fig. 3. Peaks of all samples were indexed based on monoclinic α-Cu_2Se structures with space group $C2/c$ (no. 15)[20,21,34,35] whose lattice parameter was consistent with those calculated by HR-TEM analysis in Fig. 2(b). The lattice parameters[34] a = 7.1379 Å, b = 12.3823 Å, c = 27.3904 Å, and β = 94.308° (Fig. 3(b)) were constant for the C_{60}/Cu_2Se nanocomposite with various C_{60} contents, which suggests that the C_{60}s are dispersed as a separate phase instead of reacting with the Cu_2Se.

The electrical properties of the C_{60}/Cu_2Se nanocomposites are plotted in Fig. 4. The electrical transport properties showed metallic behavior, which is typical of heavily doped thermoelectric semiconductors. The slight variation of temperature dependence around 350–400 K is clear evidence for the phase transition of Cu_2Se from monoclinic to cubic, consistent with previous reports.[20,22,35] The electrical conductivities of the C_{60}/Cu_2Se nanocomposites were less than that of pure Cu_2Se for all temperatures. As shown in Table S2,† the carrier concentration and mobility of the C_{60}/Cu_2Se nanocomposites were less than those of pure Cu_2Se, likely due to carrier localization by potential wells, as shown in Fig. 4(d).[15] C_{60} and Cu_2Se have

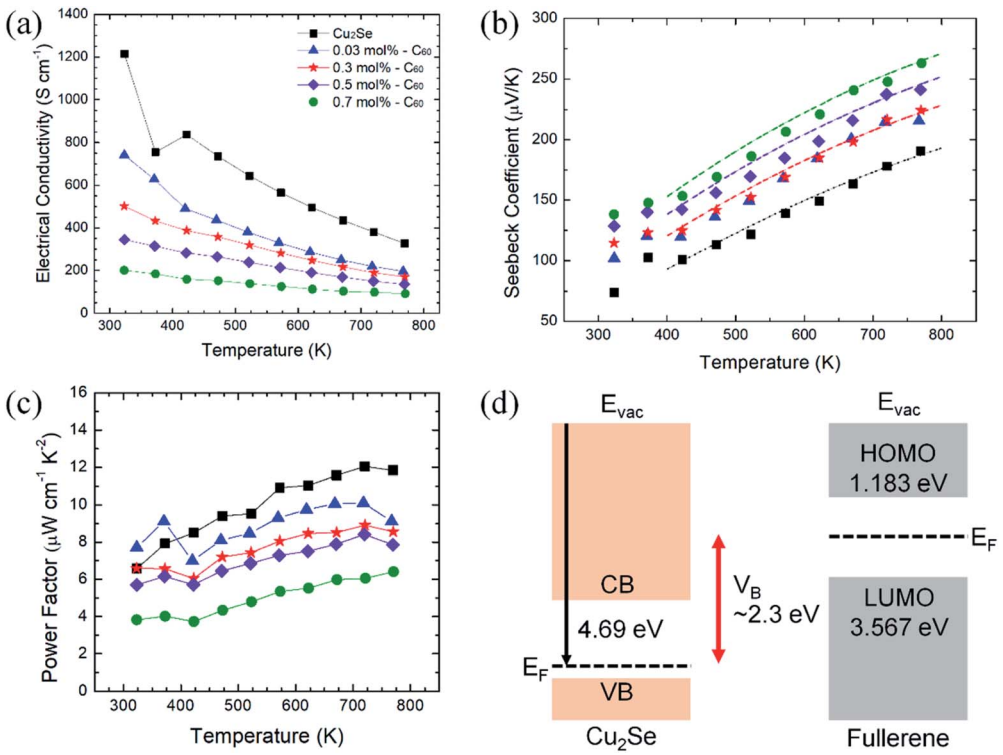

Fig. 4 Electrical properties of C_{60}/Cu_2Se nanocomposites. (a) Electrical conductivities, (b) experimental (markers) and calculated (dot-dash lines) Seebeck coefficients, (c) power factors, and (d) schematics of the band structures of Cu_2Se, and C_{60}.[38]

significantly different Fermi levels. The work function of Cu_2Se is 4.69 eV,[36] whereas the HOMO and LUMO levels of C_{60} are −1.183, and − 3.567 eV, respectively.[24] Thus, the potential well depth is estimated to be around 2.3 eV, which could be the main reason for carrier localization. The Seebeck coefficient of C_{60}/Cu_2Se nanocomposites was significantly greater than that of pure Cu_2Se (Fig. 4(b)), as expected due to carrier localization. The Seebeck coefficient was calculated using the following equation from the Boltzmann transport equation:[2]

$$S = \frac{k_B}{e}\left\{\frac{\left(r+\frac{5}{2}\right)F_{r+\frac{3}{2}}(\eta)}{\left(r+\frac{3}{2}\right)F_{r+\frac{1}{2}}(\eta)} - \eta\right\} \quad (2)$$

where r is the scattering parameter, k_B is the Boltzmann constant, e is the electron charge, F is the Fermi-Dirac integral, and η is the reduced Fermi level.[2] The scattering parameter reflects the energy dependence of electron scattering time, $\tau = \tau_o E^r$. In general, electron scattering is dominated by acoustic phonons in inorganic semiconductors.[2,15,29] The scattering parameter for acoustic phonon scattering is − 0.5. To fit our experimental data from the C_{60}/Cu_2Se nanocomposites, the scattering parameters were determined to be −0.05, 0.25, and 0.5 for the 0.3, 0.5, and 0.7 mol% C_{60}/Cu_2Se nanocomposites, respectively. An increase of the scattering parameter indicates that the slope of the $E\tau(E)D(E)$ term in eqn (1) is large, which results in enhancement of the Seebeck coefficient.[16] This result is clear evidence for carrier localization. The embedded C_{60}s change the scattering mechanism of electrons. As shown in Fig. 4(b), the Seebeck coefficient of the 0.7 mol% C_{60}/Cu_2Se nanocomposite was enhanced by around 43% compared to that of pure Cu_2Se. Because the electrical conductivity was reduced, the power factors of the C_{60}/Cu_2Se nanocomposites were not increased.

The thermal properties are plotted in Fig. 5. The thermal conductivities of the C_{60}/Cu_2Se nanocomposites were less than that of pure Cu_2Se over the entire tested temperature range. Both electron thermal conductivities and lattice thermal conductivities were reduced for all C_{60}/Cu_2Se nanocomposites compared to those of pure Cu_2Se. The reduction of electronic thermal conductivities is caused by reduction of electrical conductivities which are shown in Fig. 4(a). The lattice thermal conductivity reduction is due to phonon scattering by embedded C_{60} nanoparticles, and can be calculated by a relaxation time approximation:[4,28]

where v_g is the group velocity of phonons, $\hbar$ is the reduced Plank's constant, x is the reduced phonon energy, θ is the Debye temperature, and τ is the phonon scattering, while the subscript c represents 'combined', U represents 'Umklapp', A represents 'alloy', and N represents 'normal'.

The experimental and calculated lattice thermal conductivities are plotted in Fig. 5(c) (calculation details are described in the ESI.†) The phonon scattering by embedded C_{60}s was considered to be defect scattering. The calculation was only based on the 0.7 mol% C_{60}/Cu_2Se nanocomposite sample. The volume fraction of C_{60} is derived from the mole fraction and size of C_{60}. The calculation results fit well with the experimental results of the 0.7 mol% C_{60}/Cu_2Se nanocomposite. To fit the experimental data, 8 nm was used as the diameter of the clustered C_{60} nanoparticles, which is consistent with TEM results shown in Fig. 2. The samples with other C_{60} amounts (0.03, 0.3, 0.5 mol%) also had low lattice thermal conductivities that were similar to that of the 0.7 mol% sample. These data indicate that additional phonon scattering can drastically reduce lattice thermal conductivity when C_{60} is embedded in Cu_2Se. For example, correlated scattering between scattered phonons by multiple C_{60} nanoparticles could additionally reduce lattice thermal conductivity.[4] M. Brewster and C. Tien[37] suggested that when $c/\lambda < 0.3$, where c is the interparticle distance and λ is the phonon wavelength, the correlated scattering effect should be considered, as interference between scattered phonons becomes important. A rough estimation (as described in the ESI†) suggests that the interparticle distances for the 0.3, 0.5, and 0.7 mol% C_{60}/Cu_2Se nanocomposites were around 5.3, 4.5, and 4.0 nm, respectively. As shown in Fig. 2, the experimentally observed value for interparticle distances was also on the few-nm scale. Considering that the dominant phonon wavelength is around 1–10 nm, some portion of phonon waves could have a c/λ value below 0.3, indicating the importance of the correlated scattering effect. Therefore, the observed lattice thermal conductivity is lower than the theoretical estimate, as shown in Fig. 5(c). Because of significant phonon scattering, the lattice thermal conductivity was around 0.25 W m^{-1} K^{-1} which is similar to the minimum thermal conductivity.[2]

$$\kappa_L = \frac{k_B}{2\pi v_g}\left(\frac{k_B T}{\hbar}\right)^3\left\{\int_0^{\frac{\theta}{T}}\frac{\tau_c x^4 e^x}{(e^x-1)^2}dx + \frac{\left[\int_0^{\frac{\theta}{T}}\frac{\tau_c}{\tau_N}\frac{x^4e^x}{(e^x-1)^2}dx\right]^2}{\int_0^{\frac{\theta}{T}}\frac{1}{\tau_N}\left(1-\frac{\tau_c}{\tau_N}\right)\frac{x^4e^x}{(e^x-1)^2}dx}\right\} \quad (3)$$

$$\frac{1}{\tau_c} = \frac{1}{\tau_N} + \frac{1}{\tau_D} + \frac{1}{\tau_U} + \frac{1}{\tau_A}$$

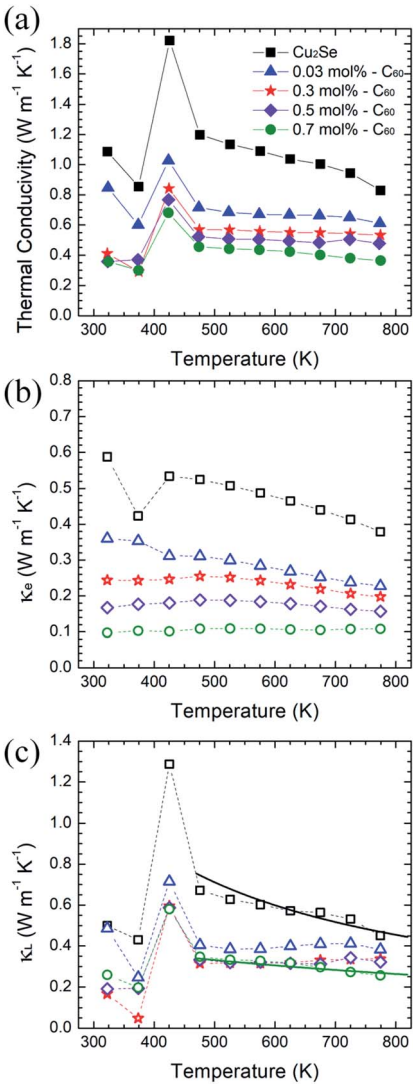

Fig. 5 Thermal properties of C_{60}/Cu_2Se nanocomposites. Experimental (markers) and calculated (solid lines) (a) total thermal conductivities, (b) electron thermal conductivities, and (c) lattice thermal conductivities.[38]

As shown in Fig. 6, the maximum zT was around 1.4 at 773 K for the 0.7 mol% C_{60}/Cu_2Se nanocomposite. The enhancement of zT was mainly caused by the synergetic effect of phonon scattering and carrier localization. The strong phonon scattering by embedded C_{60} significantly reduced lattice thermal conductivity by 40–50% over the entire tested temperature range. The energy-dependent electron scattering by potential well of C_{60} significantly reduces electrical conductivity, resulting in the reduction of electronic thermal conductivity. Through these mechanisms, incorporation of C_{60} decreases the total thermal conductivity by around 60%. Moreover, the Seebeck coefficient is enhanced by the carrier localization. By the synergetic effect of the carrier localization and phonon scattering by the embedded C_{60}s, zT is enhanced by 20–30% in C_{60}/Cu_2Se nanocomposites compared to that of pure Cu_2Se.

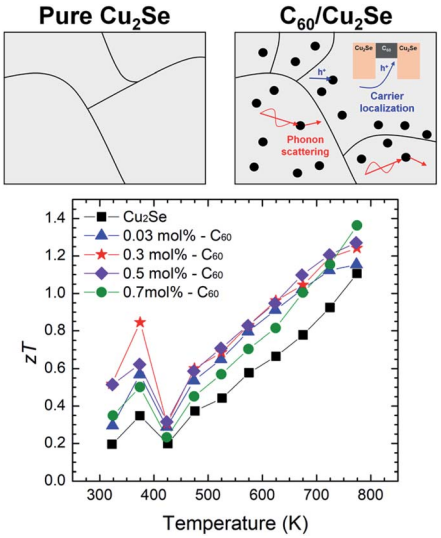

Fig. 6 Schematic comparing pure Cu_2Se and a C_{60}/Cu_2Se nanocomposite and the thermoelectric figure of merit zT as a function of temperature.[38]

Conclusion

C_{60} incorporated Cu_2Se nanocomposites were synthesized using a simple solid-state reaction. The microstructure of the C_{60}/Cu_2Se nanocomposites was different from that of pure Cu_2Se. Grain growth was suppressed in C_{60}/Cu_2Se nanocomposites because of the Zener pinning effect, showing that the nanocomposites contain more grain boundaries than pure Cu_2Se. The dispersed C_{60}s are clustered in the fullerite form around 10 nm size. They act as phonon scatterers and potential wells for holes. Due to the phonon scattering by the embedded C_{60} nanoparticles, the lattice thermal conductivity of the C_{60}/Cu_2Se nanocomposite is reduced by around 40–50% compared to that of pure Cu_2Se. The reduction of lattice thermal conductivity was analyzed quantitively using a phonon scattering model. The Seebeck coefficient was enhanced by carrier localization caused by C_{60}. Due to the difference in Fermi level between C_{60} and Cu_2Se, C_{60} can act as a potential well for carriers (holes), resulting in carrier localization (energy filtering). Through quantitative analysis using the Boltzmann transport equation, it was found that the C_{60}/Cu_2Se nanocomposites have an additional scattering process for carriers that is caused by the C_{60} nanoparticles. The additional scattering process increased the Seebeck coefficient by 43%. Through the synergetic effect of phonon scattering and carrier localization in C_{60}/Cu_2Se nanocomposites, the thermoelectric figure of merit was enhanced by 20–30% compared to that of pure Cu_2Se.

Experimental[38]

Synthesis

The precursor materials, namely, copper powder (Cu, <425 μm, 99.5%), selenium pellets (Se, <5 mm, >99.99%), and fullerene powder (C_{60}, 98%) were obtained from Sigma-Aldrich. The mixture of raw materials was sealed in a quartz tube and loaded

in a furnace, where the temperature was slowly increased to 673 K in 6 hours and then held for 2 hours. The reaction was carried out at a temperature of 1073 K for 5 days, and the samples were naturally cooled to 298 K. Subsequently, the resultant ingots were ground into a powder. The fullerene (C_{60}) was added to the as-synthesized Cu_2Se powder through a simple mechanical alloy method. Fullerenes and hand ground Cu_2Se were weighed to produce accurate C_{60} contents of 0.03, 0.3, 0.5, and 0.7 mol%. Then, the mixed powders were mechanically ground using planetary ball milling for 2 hours. The pure Cu_2Se hand ground powder was also ground again using ball milling for 2 hours. In order to obtain high density samples for measurement, the ball-milled powders were consolidated into pellets by spark plasma sintering (SPS) at 723 K and under a high pressure of 85 MPa. The relative densities of C_{60}-incorporated Cu_2Se samples were 98.6–99.9% of the theoretical density.

Characterization

The crystal structures of the ball-milled products and sintered pellets were characterized by powder X-ray diffraction (PXRD), recorded on X-ray diffractometer equipment using a Cu-K_α radiation wavelength of 1.5418 Å at 40 kV and 30 mA. The diffraction data were collected at a scan rate of 2° min^{-1} with the angle ranging from 10° to 80°. The microstructures of samples were obtained by scanning electron microscopy (SEM) using a JEOL JSM-6700F at an accelerating voltage of 10 kV. Transmission electron microscopy (TEM) and high resolution TEM (HR-TEM) images were recorded on a JEOL JEM-F200 instrument.

The electrical conductivity (σ) and Seebeck coefficient (S) were measured simultaneously on a ZEM-3 (Ulvac-Riko ZEM-3). The thermal conductivity (κ) was obtained through $\kappa = D \times C_p \times \rho$, where D, C_p and ρ are the thermal diffusivity, heat capacity, and mass density, respectively. The thermal diffusivity (D) was measured using an LFA 457 (NETZSCH). The heat capacity (C_p) was obtained from the literature.[36] The Archimedes method was performed to calculate the mass density (ρ). The Hall coefficient was obtained using a physical property measurement system (PPMS 16T, Quantum Design) with magnetic field ranging from −9 T to 9 T.

Calculation of Seebeck coefficient and lattice thermal conductivity

The calculation of the Seebeck coefficient is based on eqn (2) in the main text. The temperature-dependence of the Fermi level position is used as fitting parameter to calculate the Seebeck coefficient of pure Cu_2Se. The Seebeck coefficient for C_{60}/Cu_2Se nanocomposites is fitted by changing the scattering parameter.

The calculation of lattice thermal conductivity is based on the Callaway model, as described in eqn (3). The relaxation time for the defect (embedded C_{60}) is obtained by methods reported in the literature.[3] (A detailed process is described in the ESI.†)

Conflicts of interest

There are no conflicts to declare.

Acknowledgements

This work was supported by the National Research Foundation of Korea (NRF) grant funded by the Korea government (MSIT) (NRF-2018R1A2B2005455).

References

1 D. M. Rowe, *CRC Handbook of Thermoelectrics*, CRC Press, 1995.
2 G. Chen, *Nanoscale Energy Transport and Conversion*, Oxford university press, New york, 2005.
3 W. Kim and A. Majumdar, *J. Appl. Phys.*, 2006, **99**, 084306.
4 W. Kim, J. Zide, A. Gossard, D. Klenov, S. Stemmer, A. Shakouri and A. Majumdar, *Phys. Rev. Lett.*, 2006, **96**, 045901.
5 W. Kim, R. Wang and A. Majumdar, *Nano Today*, 2007, **2**, 40–47.
6 K. Biswas, J. He, Q. Zhang, G. Wang, C. Uher, V. P. Dravid and M. G. Kanatzidis, *Nat. Chem.*, 2011, **3**, 160–166.
7 K. Biswas, J. Q. He, G. Y. Wang, S. H. Lo, C. Uher, V. P. Dravid and M. G. Kanatzidis, *Energy Environ. Sci.*, 2011, **4**, 4675–4684.
8 J. He, J. Androulakis, M. G. Kanatzidis and V. P. Dravid, *Nano Lett.*, 2011, **12**, 343–347.
9 L. D. Zhao, J. Q. He, C. I. Wu, T. P. Hogan, X. Y. Zhou, C. Uher, V. P. Dravid and M. G. Kanatzidis, *J. Am. Chem. Soc.*, 2012, **134**, 7902–7912.
10 L. D. Zhao, J. Q. He, S. Q. Hao, C. I. Wu, T. P. Hogan, C. Wolverton, V. P. Dravid and M. G. Kanatzidis, *J. Am. Chem. Soc.*, 2012, **134**, 16327–16336.
11 A. Banik and K. Biswas, *J. Mater. Chem. A*, 2014, **2**, 9620–9625.
12 H. Wang, J.-H. Bahk, C. Kang, J. Hwang, K. Kim, J. Kim, P. Burke, J. E. Bowers, A. C. Gossard, A. Shakouri and W. Kim, *Proc. Natl. Acad. Sci. U. S. A.*, 2014, **111**, 10949–10954.
13 W. H. Nam, B. B. Kim, Y. S. Lim, K. S. Dae, W. S. Seo, H. H. Park and J. Y. Lee, *Nanoscale*, 2017, **9**, 12941–12948.
14 K. Q. Zhang, H. C. Wang, W. B. Su, T. Wang, X. Wang, T. T. Chen, T. C. Huo, F. Dang, M. Y. Dong, C. L. Wang, B. B. Dong and Z. H. Guo, *J. Phys. D: Appl. Phys.*, 2020, **53**, 245501.
15 D. Narducci, E. Selezneva, G. Cerofolini, S. Frabboni and G. Ottaviani, *J. Solid State Chem.*, 2012, **193**, 19–25.
16 M. Zebarjadi, K. Esfarjani, M. S. Dresselhaus, Z. F. Ren and G. Chen, *Energy Environ. Sci.*, 2012, **5**, 5147–5162.
17 J. H. Yingshi Jin, H. Mi-Kyung, W. Shon, R. Jong-Soo and K. Sung-Jin, *ACS Appl. Mater. Interfaces*, 2020, **12**, 36589–36599.
18 H. L. Liu, X. Shi, F. F. Xu, L. L. Zhang, W. Q. Zhang, L. D. Chen, Q. Li, C. Uher, T. Day and G. J. Snyder, *Nat. Mater.*, 2012, **11**, 422–425.
19 H. L. Ping Lu, X. Yuan, F. Xu, X. Shi, K. Zhao, W. Qiu, W. Zhang and L. Chen, *J. Mater. Chem. A*, 2015, **3**, 6901–6908.
20 H. L. Liu, X. Yuan, P. Lu, X. Shi, F. F. Xu, Y. He, Y. S. Tang, S. Q. Bai, W. Q. Zhang, L. D. Chen, Y. Lin, L. Shi, H. Lin,

X. Y. Gao, X. M. Zhang, H. Chi and C. Uher, *Adv. Mater.*, 2013, **25**, 6607–6612.
21 B. Yu, W. S. Liu, S. Chen, H. Wang, H. Z. Wang, G. Chen and Z. F. Ren, *Nano Energy*, 2012, **1**, 472–478.
22 B. Zhong, Y. Zhang, W. Q. Li, Z. R. Chen, J. Y. Cui, W. Li, Y. D. Xie, Q. Hao and Q. Y. He, *Appl. Phys. Lett.*, 2014, **105**, 123902.
23 M. Li, D. L. Cortie, J. X. Liu, D. H. Yu, S. M. K. N. Islam, L. L. Zhao, D. R. G. Mitchell, R. A. Mole, M. B. Cortie, S. X. Dou and X. L. Wang, *Nano Energy*, 2018, **53**, 993–1002.
24 R. Q. Zhang, Y. Q. Feng, S. T. Lee and C. L. Bai, *J. Phys. Chem. B*, 2004, **108**, 16636–16641.
25 S. M. Lee, R. J. Nicholls, D. Nguyen-Manh, D. G. Pettifor, G. A. D. Briggs, S. Lazar, D. A. Pankhurst and D. J. H. Cockayne, *Chem. Phys. Lett.*, 2005, **404**, 206–211.
26 V. A. Kulbachinskii, V. G. Kytin, M. Y. Popov, S. G. Buga, P. B. Stepanov and V. D. Blank, *J. Solid State Chem.*, 2012, **193**, 64–70.
27 D. G. Zhao, J. A. Ning, D. Wu and M. Zuo, *Materials*, 2016, **9**, 629.
28 W. Kim, S. L. Singer, A. Majumdar, J. M. O. Zide, D. Klenov, A. C. Gossard and S. Stemmer, *Nano Lett.*, 2008, **8**, 2097–2099.
29 S. V. Faleev and F. Leonard, *Phys. Rev. B: Condens. Matter Mater. Phys.*, 2008, **77**, 214304.
30 A. Pakdel, Q. S. Guo, V. Nicolosi and T. Mori, *J. Mater. Chem. A*, 2018, **6**, 21341–21349.
31 G. Couturier, R. Doherty, C. Maurice and R. Fortunier, *Acta Mater.*, 2005, **53**, 977–989.
32 D. K. Chen, T. Ghoneim and Y. Kulkarni, *Appl. Phys. Lett.*, 2017, 111.
33 J. I. Tapia, E. Larios, C. Bittencourt, M. J. Yacaman and M. Quintana, *Carbon*, 2016, **99**, 541–546.
34 M. D. L. Gulay, O. Strok and A. Pietraszko, *Chem. Met. Alloys*, 2011, **4**, 200–205.
35 S. Ballikaya, H. Chi, J. R. Salvador and C. Uher, *J. Mater. Chem. A*, 2013, **1**, 12478–12484.
36 R. Nunna, P. F. Qiu, M. J. Yin, H. Y. Chen, R. Hanus, Q. F. Song, T. S. Zhang, M. Y. Chou, M. T. Agne, J. Q. He, G. J. Snyder, X. Shi and L. D. Chen, *Energy Environ. Sci.*, 2017, **10**, 1928–1935.
37 M. Q. Brewster and C. L. Tien, *J. Heat Transfer*, 1982, **104**, 573–579.
38 Y. Jin, *Synthesis and Characterization of Cu2Se-based Nanostructured Materials and Their Thermoelectric Properties*, Ewha Womas University, 2020.
39 T. Chen, H. Wang, W. Su, X. Wang, F. Mehmood, K. Zhang, T. Huo and C. Wang, Thermoelectric performance of Dy/Y co-doped $SrTiO_3$ ceramic composites with submicron $A_2Ti_2O_7$ (A = Dy, Y) pyrochlore, *J. Phys. D: Appl. Phys.*, 2021, **54**(15), 155501.
40 X. Wang, H. Wang, W. Su, T. Wang, M. A. Madre, J. Zhai, T. Chen, A. Sotelo and C. Wang, A novel multilayer composite structured thermoelectric module with high output power, *J. Mater. Chem. A*, 2020, **8**, 3379–3389.